Synthetic Metals 221 (2016) 48–54

Contents lists available at ScienceDirect

Synthetic Metals

journal homepage: www.elsevier.com/locate/synmet

Ambipolar small molecular semiconductor-based heterojunction diode

R.O. Ocaya[a], Mehmet Özdemir[b], Resul Özdemir[b], Ahmed Al-Ghamdi[c], Hakan Usta[b], W.A. Farooq[d], F. Yakuphanoglu[c,e,*]

[a] Department of Physics, University of the Free State, South Africa
[b] Department of Materials Science and Nanotechnology Engineering, Abdullah Gül University, Kayseri, Turkey
[c] Department of Physics, Faculty of Science, King Abdulaziz University, Jeddah 21589, Saudi Arabia
[d] Physics and Astronomy Department, College of Science, King Saud University, Riyadh, Saudi Arabia
[e] Department of Physics, Faculty of Science, Firat University, Elazig 23169, Turkey

ARTICLE INFO

Article history:
Received 30 August 2016
Received in revised form 29 September 2016
Accepted 1 October 2016
Available online 15 October 2016

Keywords:
Organo-metal diode
Schottky diode
Photodiode
2OD-TIFDKT
Polymer diode

ABSTRACT

A heterojunction diode based on an ambipolar organic semiconductor 2,8-bis(5-(2-octyldodecyl)thien-2-yl)indeno[1,2-*b*]fluorene-6,12-dione (2OD-TIFDKT) was fabricated on p-Si using a drop-casting technique. The current–voltage and capacitance-voltage characteristics of Al/2OD-TIFDKT/p-Si/Al devices with aluminized contacts were investigated under dark and 100 mW/cm^2 illumination intensity. The result is a novel interface-state controlled diode device that is shown to be rectifying. In the forward, bias it has a current that depends on the illumination intensity at constant bias, showing potential application in low-power solar cell application. In the reverse bias, it has a response that depends on the illumination intensity regardless of the applied reverse bias. This suggests a potential use as a sensor in photoconductive applications. Between 0 and 0.7 V forward bias, the ideality factor, series resistance and barrier height average at 2.35, 67.6 kΩ and 0.842 eV, respectively, regardless of illumination.

1. Introduction

Organic semiconductors consisting of π-conjugated small molecules (π-SM) have emerged over the past few decades as promising candidates for application in low-cost, flexible, and large area organic devices. Such devices include, but are not limited to organic light-emitting diodes (OLED), organic thin-film transistors (OTFT), organic photovoltaics (OPV), light-emitting transistors (OLET), sensors and large-area integrated circuits. These devices, because of their inherently low electron and hole mobilities, are not intended to compete with silicon-based technologies, but are desired to be lower-cost alternatives. At the same time, significant developments continue to boost organic device performance due to improved synthetic methods, optimization techniques and device engineering [1]. In contrast to larger π-conjugated macromolecular systems, π-SMs have the advantages of easier synthesis, better purity and yield, good solubility in common organic solvents and better thin-film crystallinity. These traits lead to good reliability and device fabrication reproducibility [2]. One current design approach for semiconducting organic molecules is to attempt the realization of a good balance between solution processability, highest occupied molecular orbital (HOMO)/lowest unoccupied molecular orbital (LUMO) energies, optical band gaps and actual device packaging and metallization [1,2]. With the continuing rapid development of new semiconducting organic materials, the need to better understand and rationalize electronic structure, charge transport and organic molecule/metal interfaces become increasingly important [3]. With the emergence of organic semiconductors in optoelectronic devices, metal/organic interfaces were initially studied in the context of the established metal/semiconductor interface theory developed by Schottky-Mott for ideal metal/inorganic semiconductor interfaces. Recent studies have revealed that such interfaces are dominated by large dipole interactions that lead to significant Fermi-level pinning and manipulation barrier height [4]. In order to realize optimized high-performance devices, lowered charge-injection barrier height with minimized localized trap states at the organo-metal interface is needed. Ideally, the organic-metal interface should offer low charge injection barriers for Ohmic contact, which depends on the difference in energy between the metal work function and the HOMO level for hole injection or LUMO level for electron injection. This condition can be closely approached for organic-metal interfaces if there is direct contact

* Corresponding author at: Department of Physics, Faculty of Science, Firat University, Elazig 23169, Turkey.
E-mail address: fyhan@hotmail.com (F. Yakuphanoglu).

http://dx.doi.org/10.1016/j.synthmet.2016.10.001
0379-6779/

between the metal and the Π-electrons in the conjugated small molecule. The metal atoms are evaporated and condensed onto the organic film, where diffusion of metal atoms up to several nanometers of the p organic surface can occur during deposition [5]. However, the exact nature of the interface relies on the deposition method, which controls the surface morphology. The work of Liu et al. [1] also suggests that engineering the contact surface with an ultra-thin, insulating layer before the deposition of π-SMs, the performance of the device could be enhanced substantially. Specifically, they studied the role of 0–6 nm thicknesses of Si_3N_4 for two different organic compounds. Their findings suggest that the onset of various device behaviors-from rectifying to quasi-Ohmic to tunneling-could be controlled by tuning the insulator thickness, which is in agreement with the theory of Fermi-level pinning or de-pinning [6]. The distribution of the localized states close to the organic-metal interface was found to change due to the improved protection of the organic-film from physical interference during metallization. In addition, the improved modulation of the charge injection led to reduced barrier height. The use of Si_3N_4 was motivated by the need to avoid oxygen during a thermally activated deposition process, which could lead to oxidation artifacts arising from the organic compound. Also, the wider band gap of the insulator is chosen to be far from the HOMO/LUMO energies thereby eliminating charge injection into these levels [1]. On the account of the band gap of SiO_2, (∼9 eV), which is much higher that of metal oxides and Si_3N_4 (∼5.3 eV) would be ideal [7]. However, the aforementioned need to avoid oxygen precludes it. Another currently held general principle of organic molecule design for practical applications is to attempt to achieve lower band gap and to enhance π-conjugation by engineering donor-acceptor molecular architectures while minimizing the torsional forces between the rings coupling the π-electron deficient acceptors and the π-electron rich donor moieties [8–11]. The role of substituents such as chlorine has also been investigated by Ryu et al. [12]. Their findings suggest that such substitutions may extend the application of organic semiconductors in optoelectronic devices by enhancing physicochemical and optoelectronic properties through the band gap and relative positions of HOMO/LUMO energies. This also has direct implications to the possible metallization contacts. Some effects of annealing on the thermal and electrical properties were investigated by Wang et al. [13], who found that annealing small organic molecules at temperatures between 24 °C and 140 °C led to a gradual increase in the field effect mobility while shifting the threshold voltage from positive to negative. Some efforts have been spent by others to functionalize the organic–metal interface through work-function modification by employing higher ordering of self-assembled molecular mono-layers [14]. In this paper, we report on the synthesis and application of an organic small molecule based on an indeno[1,2-*b*]fluorene-6,12-dione-thiophene ladder-type ambipolar building block, which demonstrates good charge transport ability and device stability. The molecule is designed based on the repositioning the β-substituents to a molecular terminal referred to as α, ω-disubstitution, which has improved the stereochemistry by enhancing the π-core planarity of the semiconductor backbone through reduced steric interactions. The resulting ambipolar organic compound is 2,8-bis(5-(2-octyldodecyl)thien-2-yl)indeno[1,2-*b*]fluorene-6,12-dione (2OD-TIFDKT), which has been recently reported as an ambipolar semiconductor in OTFTs with good charge transport characteristics ($\mu_e = 0.12\ cm^2/Vs$ $\mu_h = 0.02\ cm^2/Vs$). We present the results of the fabrication and measurements of a novel metalized rectifying 2OD-TIFDKT/p-Si junction diode, which has few precedents and has a potential use as in sensor applications.

2. Experimental

2.1. Synthesis of ambipolar 2OD-TIFDKT

Scheme 1

2.2. Materials and methods

The reagents used in this synthetic work were acquired from commercial sources and used as received. Vacuum/nitrogen manifold was used for the reactions that will be carried out under N_2 and for drying processes. ^1H NMR (400 MHz) and ^{13}C NMR (100 mHz) spectra were recorded on a Bruker 400 spectrometer. LecoTruspec Micro model instrument and Bruker Microflex LT MALDI-TOF-MS Instrument were used for elemental and MALDI-TOF analyses.

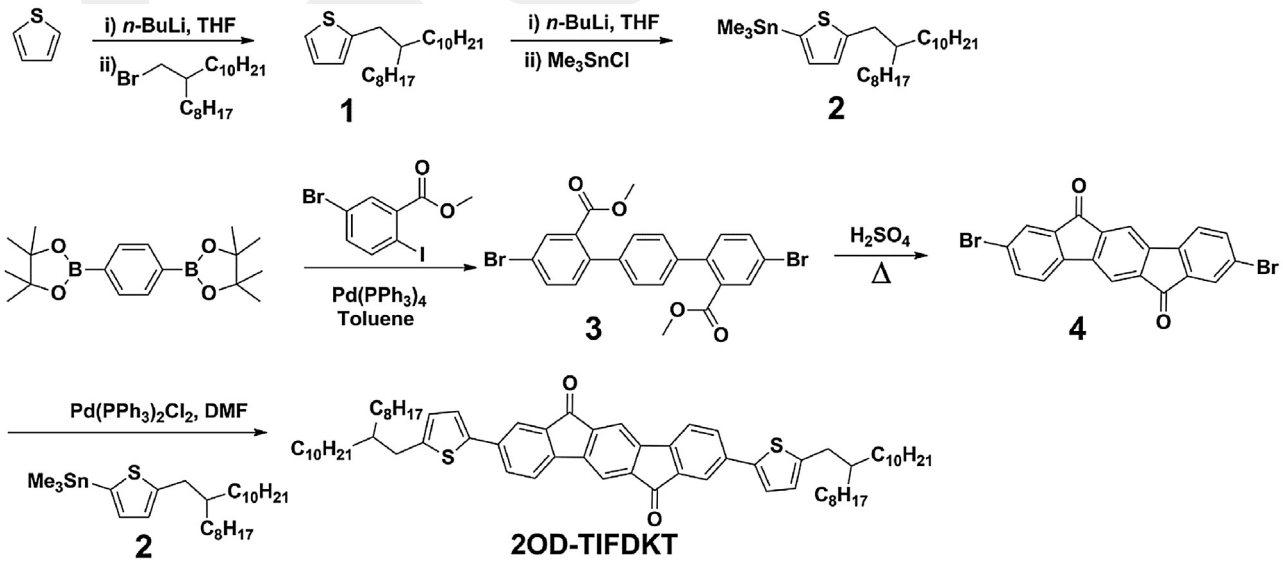

Scheme 1. Synthesis of 2,8-bis(5-(2-octyldodecyl)thien-2-yl)indeno[1,2-*b*]fluorene-6,12-dione (**2OD-TIFDKT**).

2.3. Synthesis and characterizations

The synthetic route to 2OD-TIFDKT is shown in Scheme 1. In addition, the details for the synthesis of 2-octyldodecyl bromide is given in the following procedure:

2.3.1. Synthesis of 2-octyldodecyl bromide

The reagents 2-octyl-1-dodecanol (5.4 g, 18 mmol) and triphenylphosphine (6.84 g, 72 mmol) were dissolved in 240 mL THF in ambient, which is followed by the addition of bromine (10.8 g, 72 mmol). The resulting reaction solution was stirred at room temperature for several hours. After the reaction is completed, 3 mL of methanol was added to this mixture, and the solvent was evaporated. Then, hexane was added, the precipitate was removed by filtration, and the filtrate was concentrated to yield a crude oil. Final purification was performed by column chromatography using silica gel and hexane as the stationary phase and eluent to yield the pure product as a colorless oil (6.2 g, 95%). ^{1}H NMR (400 MHz, $CDCl_3$): δ 3.44 (2H, d, J = 4.8 Hz), 1.58 (1H, m), 1.27 (32H, m), 0.88 (6H, t, J = 6.7 Hz).

2.3.2. Synthesis of 2-(2-octyldodecyl) thiophene **(1)**

2.68 mL (6.7 mmol) of *n*-butyllithium (2.5 M in *n*-hexane) was added to a solution of thiophene (0.537 g, 6.38 mmol) in THF (10 mL) at −78 °C under nitrogen. The lithiation was performed by stirring at −78 °C for 30 min and at room temperature for 1 h, respectively, which was followed by the addition of 1-bromo-2-octyldodecane (2.44 g, 7.02 mmol) at −78 °C. Next, the reaction mixture was heated to reflux for 12 h. After the reaction was completed, the reaction mixture was quenched with water and the product was extracted into an organic phase (chloroform). The crude product was obtained after evaporation to dryness, which was purified by column chromatography using silica gel and hexane as the stationary phase and eluent, respectively. The pure product was obtained as a colorless oil (1.28 g, 55.0%). ^{1}H NMR (400 MHz, $CDCl_3$): δ 0.89 (m, 6H), 1.27-1.33 (m, 33H), 2.76 (d, 2H, J = 6.8 Hz),6.76 (d, 1H, J = 3.4 Hz), 6.92 (dd, 1H, J = 5.2 Hz, J = 3.4 Hz), 7.13 (d, 1H, J = 5.2 Hz).

2.3.3. Synthesis of 2-(2-octyldodecyl)-5-trimethylstannylthiophene **(2)**

1.29 mL (3.22 mmol) of *n*-butyllithium (2.5 M in *n*-hexane) was added to a solution of 2-(2-octyldodecyl)thiophene (**1**) (1.12 g, 3.07 mmol) in THF (25 mL) at −78 °C under nitrogen. The lithiation was performed by stirring at −78 °C for 30 min and at room temperature for 1 h. To this lithiated mixture, trimethyltinchloride (0.67 g, 3.37 mmol) was added at −78 °C, and the reaction mixture was stirred overnight while warming to room temperature. The final reaction mixture was quenched with water, and the product was extracted into an organic phase (hexanes). The organic phase was washed with brine and dried over Na_2SO_4. The final pure product was obtained as a colorless oil (1.52 g, 94%). ^{1}H NMR ($CDCl_3$, 400 MHz): δ 0.35 (s, 9H), 0.91 (m, 6H), 1.25-1.33 (m, 33H), 2.80 (d, 2H, J = 6.0 Hz), 6.88 (d, 1H, J = 3.2 Hz), 7.02 (d, 1H, J = 3.2 Hz).

2.3.4. Synthesis of 4,4″-dibromo-2,2″-methoxycarbonyl-[1,1′;4′,1″] terphenyl **(3)**

The reagents 1,4-benzenediboronic acid bis(pinacol) ester (0.5 g, 1.51 mmol), methyl 2-iodo-5-bromobenzoate (1.13 g, 3.32 mmol), and Aliquat 336 (0.174 g, 0.43 mmol) were added under nitrogen to a reaction flask containing 10 mL of dry toluene. Next, tetrakis(triphenylphosphine)palladium (0.10 g, 0.09 mmol) and deaerated 1 M aqueous sodium carbonate solution (0.64 g in 6.1 mL of water) were added and the reaction mixture was heated at reflux for 2 days under nitrogen. After the reaction is completed, the mixture was cooled to room temperature and quenched with water. The product was extracted into an organic phase with hexanes and evaporated to dryness to yield the crude product. The pure product was obtained as a white solid (0.66 g, 86.0% yield) after column chromatography using silica gel and chloroform as the stationary phase and the eluent. ^{1}H NMR (400 MHz, $CDCl_3$): δ 3.71 (s, 6H), 7.32 (m, 6H), 7.67 (dd, 2H, J = 8.0 Hz and J = 2.4 Hz), 8.00 (d, 2H, 2.4 Hz).

2.3.5. Synthesis of 2,8-dibromo-indeno[1,2-b]fluorene-6,12-dione **(4)**

A mixture of **3** (0.55 g, 1.08 mmol) in 54.0 mL of 80% H_2SO_4 (prepared from 11 mL of H_2O and 44 mL of concentrated (98%) H_2SO_4) was stirred at 120 °C for 1 day. Next, the resulting reaction suspension is poured into ice-water mixture to yield a dark red solid. The crude product was then collected by filtration, and washed with water and saturated $NaHCO_3$ solution, and methanol, respectively. Since the solubility of 4 in common organic solvents is very low, the crude product was purified by high vacuum-based thermal gradient sublimation (2×10^{-5} Torr). The pure product was obtained as a cherry red crystalline solid (0.384 g, 80% yield). m.p. > 390 °C. Anal.calcd. for $C_{20}H_8O_2Br_2$: C, 54.58; H, 1.83 Found: C, 54.70; H, 1.96.

2.3.6. Synthesis of 2,8-bis(5-(2-octyldodecyl)thien-2-yl)indeno[1,2-b] fluorene-6,12-dione (2OD-TIFDKT)

2,8-dibromo-indeno[1,2-*b*]fluorene-6,12-dione (**4**) (0.546 g, 1.24 mmol), 2-trimethylstannyl-5-(2-octyldodecyl)thiophene (**2**) (1.44 g, 2.73 mmol), and $Pd(PPh_3)_2Cl_2$ (0.087 g, 0.124 mmol) were added under nitrogen to a reaction flask containing 60 mL of anhydrous DMF. Afterward, the reaction mixture was heated at 125 °C for 1 day. After the reaction was completed, the mixture was cooled to room temperature and evaporated to dryness. After filtration with methanol, the dark crude solid was obtained by washing with methanol, acetone, and hexanes respectively. The pure product was obtained as a dark green solid (0.50 g, 40% yield) after column chromatography using silica gel and $CHCl_3$/hexanes (7:3) as the stationary phase and the eluent. m.p. 135–136 °C. ^{1}H NMR (400 MHz, $CDCl_3$): δ 0.90 (m, 6H), 1.28–1.31 (m, 33H), 2.74 (d, 2H, J = 6.4 Hz), 6.68 (d, 1H, J = 3.2 Hz), 7.12 (d, 1H, J = 3.6 Hz), 7.38 (d, 1H, J = 7.6 Hz), 7.60 (m, 2H), 7.70 (s, 1H).^{13}C NMR (100 MHz, $CDCl_3$): δ 14.1, 22.7, 26.6, 29.3, 29.4, 29.7, 29.8, 29.9, 30.0, 31.9, 33.2, 34.7, 40.0, 115.7, 120.8, 120.9, 123.5, 126.4, 131.3, 134.6, 136.1, 139.4, 140.2, 141.2, 145.4, 145.5, 192.5. IR (KBr): 1710 cm^{-1} (C=O Stretching). MS (MALDI-TOF) m/z (M^+): calcd. for $C_{68}H_{94}O_2S_2$: 1008, found: 1009 $[M+H]^+$. Anal.calcd. for $C_{68}H_{94}O_2S_2$: C, 81.06; H, 9.40, Found: C, 81.31; H, 9.52.

2.4. Diode fabrication and characterization

2OD-TIFDKT powder sample was dissolved in water and stirred to obtain a clear solution. For the fabrication of the diode, firstly, an ohmic contact was prepared on p-type silicon. P-type silicon substrate was cleaned by chemical cleaning procedure. Then, Al metal was evaporated on p-type silicon substrate to obtain Al dots. After evaporation process, p-Si/Al wafer was annealed at 570 °C for 5 min. After ohmic contact preparation procedure, the solution of 2OD-TIFDKT sample was drop casted onto p-type silicon substrate having ohmic contact and dried to obtain a solid film. The top contacts were prepared by thermal evaporating of aluminum onto film as dots having 1 mm diameter. Fig. 2 shows the construction of the Au/2OD-TIFDKT/p-Si/Al diode. The diode contact area was found to be 3.14×10^{-2} cm^2. The electrical characterizations of the diodes were performed using a FYtronix Solar IV characterization system (Fig. 1b,).

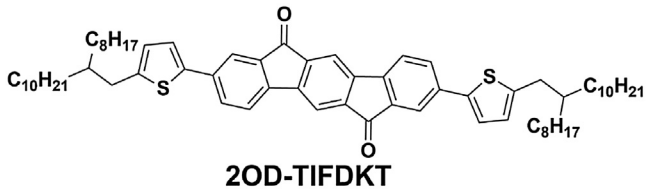

Fig. 1. Chemical structure of 2,8-bis(5-(2-octyldodecyl)thien-2-yl)indeno[1,2-*b*]fluorene-6,12-dione (**2OD-TIFDKT**).

3. Results and discussion

Fig. 3 shows the Al/2OD-TIFDKT/p-Si/Al diode I–V characteristics under dark and 100 mW/cm^2 illumination. The method of Cheung & Cheung was used to extract the diode parameters [15–17].

In the method

$$\frac{dV}{dlnI} = R_sI + n\left(\frac{kT}{q}\right) \quad (1)$$

and

$$H(I) = R_sI + n\Phi_b \quad (2)$$

where

$$H(I) = V - n\left(\frac{kT}{q}\right)\ln\left(\frac{I}{AA^*T^2}\right) \quad (3)$$

where Φ_B is barrier height, n is ideality factor and R_S is resistance. For a rectifying diode, thermionic emission theory [18] relates current (I) at applied bias (V) and temperature (T) by the equation

$$I = AA^*T^2\exp\left(-\frac{q\Phi_b}{kT}\right)\exp\left[\frac{q(V - IR_s)}{nkT}\right] \quad (4)$$

where q is electronic charge, A is device area, k is Boltzmann constant. The effective Richardson's constant A^* is 32A/cm^{2}K^2 for p-Si [19]. Fig. 3 shows diode rectifying behavior. The forward bias region depicts three distinct regions, suggesting that the device parameters such as ideality factor, resistance and barrier height depend on the applied bias. This further suggests the dependence on interface properties and barrier inhomogeneities [20]. In addition, recent studies of electron transfer mechanisms highlight the need to better understand the interface chemistry [21], particularly since electron and hole mobilities for such devices are already lower due to dependence on the interfaces and employed processing method. This is certainly the case if established Schottky diode methods such as Shockley's equation are to be extensible to the new organic-metal based devices. At the same time, it is well understood in the literature that the I–V curves of organic photovoltaics such as solar cells analyzed through Shockley's equation yield ideality factors, parallel device resistance and photo-currents that do not necessarily convey a physical meaning [22]. Therefore, some caution is needed when interpreting the analytical results. Table 1 shows the diode parameters using the Cheung-Cheung method. The data in Table 1 suggests that generally ideality factor increases while barrier height falls with applied forward bias. However, in the low forward bias region between 0.2 V and 0.7 V both the ideality factor and the barrier height are nearly constant at ~2.35 and ~0.842 eV, respectively for both dark and 100 mW/cm^2 illumination. The ideality factor of the

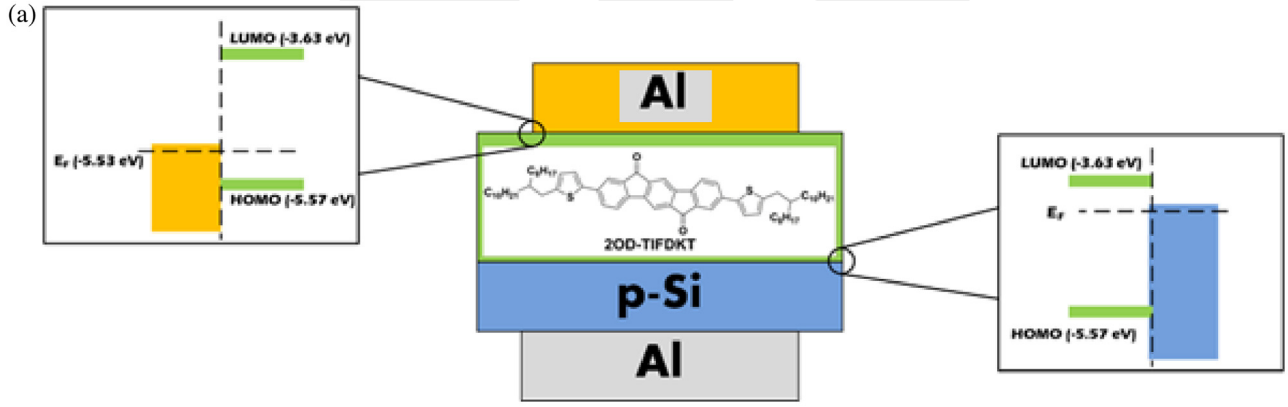

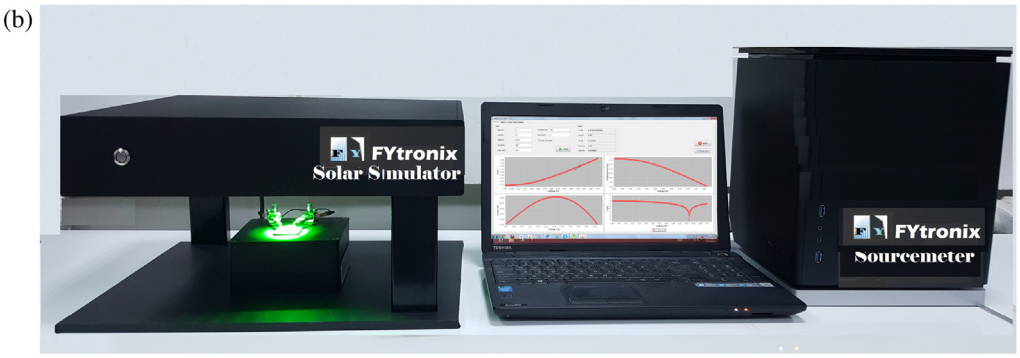

Fig. 2. a) Construction of the Al/2OD-TIFDKT/p-Si/Al diode b) FYtronix solar IV characterization system.

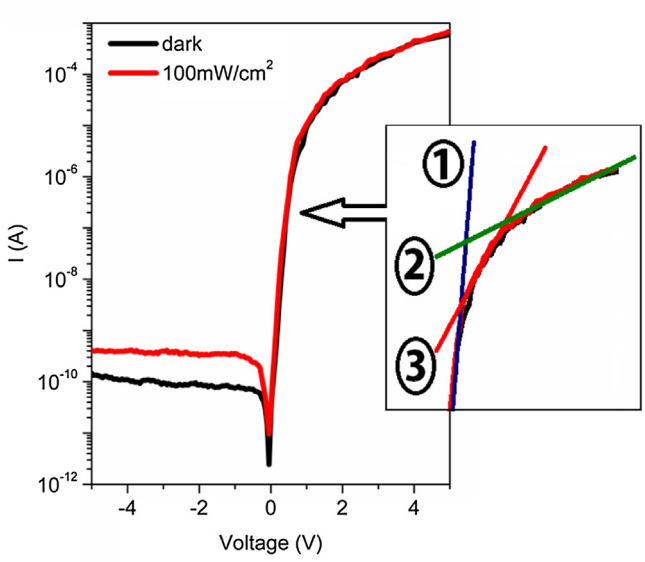

Fig. 3. I–V characteristics of Al/2OD-TIFDKT/p-Si/Al diode under dark and 100 mW/cm^2 illumination. The forward characteristics magnified in the inset, show three distinct regions 1–3. The reverse characteristics show that the diode has a photoresponse.

diode is higher than unity. The higher ideality factor of the diode is resulted from the interface states and series resistance.

However, the diode resistance is observed to drop to less than half of its dark value of 67.6 kΩ. This suggests possible application as a photovoltaic cell in this region, since the output power is higher at increased illumination at nearly constant open-circuit diode voltage. It may be expected that in this region, the diode behavior is closer to the ideal thermionic emission model portrayed by Eq. (4). The reverse bias region shows photoconductive behavior, although intensities between dark and 100 mW/cm^2 would be needed to establish the exact nature of the illumination dependence, for instance using the power law suggested by Soylu et al. [23].

Impedance spectroscopy on the device relied on capacitance-voltage measurements on the Al/2OD-TIFDKT/p-Si/Al diode on the 100 kHz − 1 MHz frequency range. Fig. 4 shows the C-V plots for the diode.

Table 2 shows the determined intrinsic carrier density (N_i), built in potential (V_{bi}), and barrier height (Φ_B), using the C-V method on the Al/2OD-TIFDKT/p-Si/Al diode. The calculated N_i shows higher variance over the frequencies used unlike suggesting sensitivity to the measurement frequency. Both V_{bi} and Φ_B show lower sensitivity to characterization frequency, averaging 2.18 ± 0.02 V and 1.53 ± 0.05 eV respectively. The calculated barrier height is approximately twice the maximum from the I–V method in Region 1. Barrier heights calculated using the two methods are known to often differ markedly [24].

Fig. 5(a) and (c) show measured capacitance and conductance measured against the applied voltage. Fig. 5(b) and (d) show the capacitances and conductance adjusted for the effects of diode

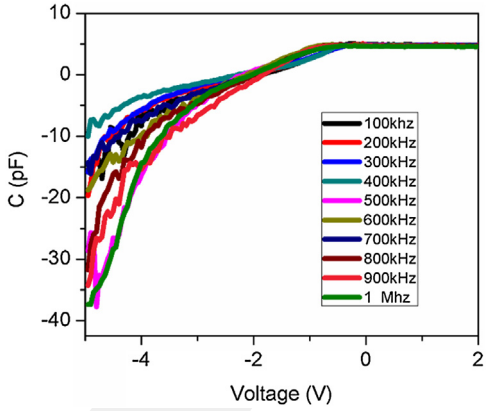

Fig. 4. C-V measurements on the Al/2OD-TIFDKT/p-Si/Al diode.

series resistance (R_S). These plots exhibit low and high-frequency dependence indicating the existence of interface states. It can be seen that the conductance increases rapidly with the frequency. The series resistance of the diode was directly measured using an impedance analyzer and it was shown in Fig. 6.

The series resistance of the diode can be determined by the following equation [25–27]

$$R_S = \frac{(G_m/\omega C_m)^2}{1 + (G_m/\omega C_m)^2} G_m \tag{5}$$

The peaks in the plot shift towards higher positive bias voltage as frequency is increased. The peak intensity decreases frequency, suggesting that the interface states change are frequency dependent. At lower frequencies interface states easily follow the AC signal resulting in excess capacitance in contrast to higher frequencies, leading to decreased contribution to interface state capacitance [28,29]. C-V and G-V measurements therefore need series resistance compensation before parameter extraction using impedance spectroscopy. The adjusted capacitance (C_{ADJ}) and conductance (G_{ADJ}) are expressed [30] as

$$C_{ADJ} = \frac{\left[G_m^2 + (\omega C_m)^2\right]}{a^2 + (\omega C_m)^2} C_m \tag{6}$$

Table 2
Extracted parameters of the Al/2OD-TIFDKT/p-Si/Al diode C-V using the C-V method.

f (kHz)	N_i (/cm^3)	V_{bi} (V)	Φ_B (eV)
100	2.17E + 08	1.97	1.01
200	7.18E + 09	2.18	1.61
300	3.57E + 08	2.28	1.63
400	4.47E + 06	2.38	1.61
500	7.68E + 08	2.28	1.66
600	3.25E + 09	2.23	1.64
700	2.87E + 10	2.15	1.61
900	1.78E + 10	1.97	1.43

Table 1
Al/2OD-TIFDKT/p-Si/Al diode parameters from the Cheung-Cheung method.

	Region 1			Region 2			Region 3		
Intensity (mW/cm^2)	n	R_s (kΩ)	Φ (eV)	n	R_s (kΩ)	Φ (eV)	n	R_s (kΩ)	Φ (eV)
Dark	2.2	67.6	0.860	6.1	14.2	0.705	19.5	3.81	0.586
100	2.5	30.9	0.824	11.4	5.3	0.641	39.4	1.58	0.534

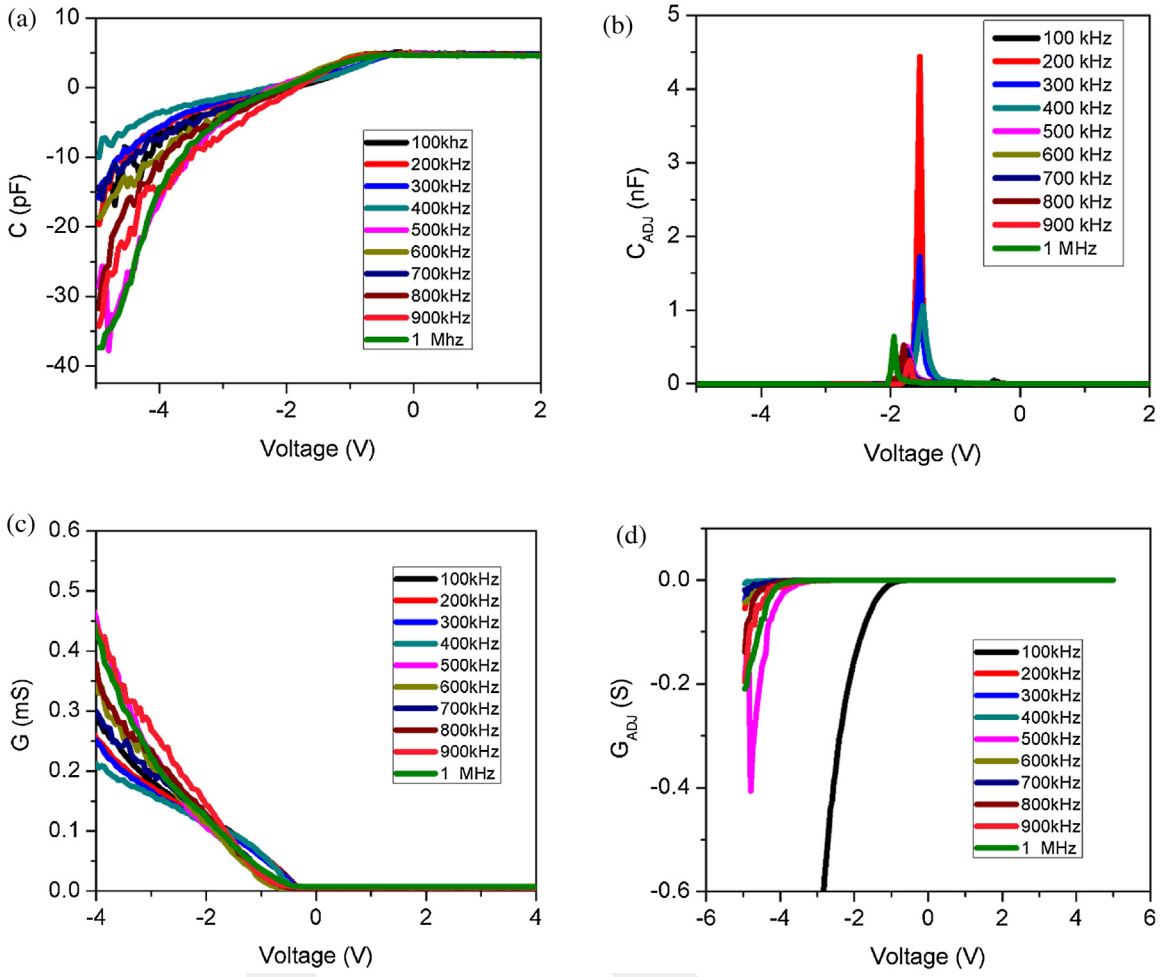

Fig. 5. Plots of the capacitance/adjusted capacitance and conductance/adjusted conductance using 100 kHz–1 MHz frequencies on the Al/2OD-TIFDKT/p-Si/Al diode.

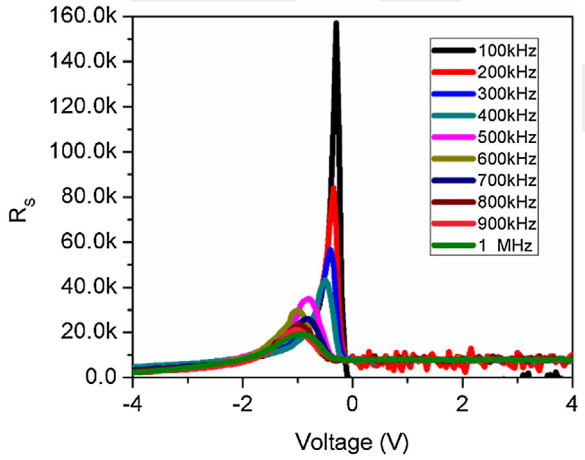

Fig. 6. A plot of the series resistance of the Al/2OD-TIFDKT/p-Si/Al diode as a function of frequency and applied voltage.

$$G_{ADJ} = \frac{\left[G_m^2 + (\omega C_m)^2\right]}{a^2 + (\omega C_m)^2} a \tag{7}$$

where $a = G_m - \left[G_m^2 + (\omega C_m)^2\right] R_s$. Diode junction capacitance is made up of diffusion and depletion layer capacitances [26,30–32]. The depletion layer capacitance (C) is given by

$$\frac{1}{C^2} = \frac{2}{q\varepsilon_r A^2 N_i}(V_{bi} + V_r - V_{th}) \tag{8}$$

where $\varepsilon_r = 11.8\varepsilon_0$ is the effective permittivity of p-Si, A is the diode area, N_i is the non-compensated ionized acceptor density, V_{bi} is the built-in voltage, V_r is the applied reverse voltage and V_{th} is the thermal voltage. The barrier height (Φ_B) is then [33]

$$\Phi_B = V_{bi} + \frac{kT}{q}\left[1 + \ln\frac{N_V}{N_i}\right] \tag{9}$$

where $N_V \approx 1.04 \times 10^{19}\,\mathrm{cm}^{-3}$ is the valence band density of states for p-Si at 300 K. Table 2 shows the calculated built-in voltage, non-ionized acceptor density and barrier height derived from Eq. (9). Nicollian & Brews [32] outlined a method by which the interface-state densities of the diode could be estimated through measured C-V, G-V data. Their method relies on peaking in the G-V characteristics. In the present case, no peaking is observed.

4. Conclusions

The present paper presents the detailed synthesis of an organic small molecule 2,8-bis(5-(2-octyldodecyl)thien-2-yl)indeno[1,2-*b*]fluorene-6,12-dione (2OD-TIFDKT) and its application in the

fabrication of a novel new p-Si substrate diode metalized with aluminum. Al/2OD-TIFDKT/p-Si/Al exhibited a good rectifying behaviour. At low forward bias, it has a low ideality factor of ~2 and its properties can be explored through the thermionic emission theory. Between 0–0.7 V forward bias the ideality factor, series resistance and barrier height average of 2.35, 67.6 kΩ and 0.842 eV, respectively, regardless of illumination. In addition, the analysis shows that the series resistance drops under illumination at a given bias value, suggesting that the device can operate as a photovoltaic cell. In reverse bias, the illumination current is reasonably constant over a wide range of bias voltages, suggesting that the diode has a potential in photoconductive applications. Impedance spectroscopy measurements indicate that interface states govern the electrical behavior of the device, suggesting the need to better understand the nature of the interfaces within the device.

Acknowledgments

This study was supported by FIRAT University Scientific Research Projects Unit under project number: FF.15.19. The authors extend their appreciation to the International Scientific Partnership Program ISPP at King Saud University for funding this research work through ISPP# 0046.

References

[1] Z. Liu, M. Kobayashi, B.C. Paul, Z. Bao, Y. Nishi, Phys. Rev. B 82 (2010) 035311.
[2] M. Ozdemir, D. Choi, G. Kwon, Y. Zorlu, H. Kim, M.-G. Kim, S.Y. Seo, U. Sen, M. Citir, C. Kim, H. Usta, RSC Adv. 6 (2016) 212.
[3] A. Facchetti, Chem. Mater. 23 (2011) 733–758, doi:http://dx.doi.org/10.1021/cm102419z.
[4] I.G. Hill, D. Milliron, J. Schwartz, A. Kahn, Appl. Surf. Sci. 166 (2000) 354–362.
[5] D.R. Vij (ed.), Handbook of Electroluminescent Materials, IOP Series in Optics and Optoelectronics, 2004.
[6] V. Heine, Phys. Rev 138 (1965) A1689.
[7] J. Robertson, Rep. Prog. Phys. 69 (2006) 327–396.
[8] R.P. Ortiz, H. Yan, A. Facchetti, T.J. Marks, Materials 3 (2010) 1533–1558.
[9] H. Usta, M.D. Yilmaz, A.-J. Avestro, D. Boudinet, M. Denti, W. Zhao, J.F. Stoddart, A. Facchetti, Adv. Mater. 25 (2013) 4327.
[10] P. Sonar, S.P. Singh, Y. Li, Z.-E. Ooi, T.-J. Ha, I. Wong, M.S. Soh, A. Dodabalapur, Energy Environ. Sci. 4 (2011) 2288–2296.
[11] H. Usta, A. Facchetti, T.J. Marks, J. Am. Chem. Soc. 130 (2008) 8580.
[12] G.-S. Ryu, Z. Chen, H. Usta, Y.-Y. Noh, A. Facchetti, MRS Commun. (2016) 1–14, doi:http://dx.doi.org/10.1557/mrc.2016.4.
[13] X. Wang, B. Peng, P. Chan, MRS Adv. (2016) 1–7, doi:http://dx.doi.org/10.1557/adv.2016.148.
[14] R. Pfattner, M. Mas-Torrent, C. Moreno, J. Puigdollers, R. Alcubilla, I. Bilotti, E. Venuti, A. Brillante, V. Laukhin, J. Veciana, C. Rovira, J. Mater. Chem. 22 (2012) 16011–16016, doi:http://dx.doi.org/10.1039/c2jm32925e.
[15] S.K. Cheung, N.W. Cheung, Appl. Phys. Lett. 85 (1) (1986).
[16] D.T. Phan, R.K. Gupta, G.S. Chung, A.A. Al-Ghamdi, O.A. Al-Hartomy, F. El-Tantawy, F. Yakuphanoğlu, Sol. Energy 86 (2012) 2961–2966.
[17] R.O. Ocaya, A. Dere, H. Tuncer, A.A. Al-Ghamdi, D.C. Sari, F. Yakuphanoglu, Synth. Met. 209 (2015) 164–172, doi:http://dx.doi.org/10.1016/j.synthmet.2015.07.016.
[18] E.H. Rhoderick, R.H. Williams, Metal-Semiconductor Contacts, second ed., Clarendon Press, Oxford, 1988.
[19] R.K. Gupta, R.A. Singh, Mater. Chem. Phys. 86 (2004) 279–283.
[20] F. Yakuphanoglu, B.F. Senkal, A. Sarac, J. Electron. Mater. 37 (2008) 930.
[21] X. Liu, J.M. Cole, P.G. Waddell, T.-C. Lin, J. Radia, A. Zeidler, J. Phys. Chem. A 116 (2012) 727–737, doi:http://dx.doi.org/10.1021/jp209925y.
[22] U. Würfel, D. Neher, A. Spies, S. Albrecht, Nat. Commun. 6 (2015) 6951, doi:http://dx.doi.org/10.1038/ncomms7951.
[23] M. Soylu, M. Cavas, A.A. Al-Ghamdi, Z.H. Gafer, F. El-Tantawy, F. Yakuphanoğlu, Sol. Energy Mater. Sol. Cells 124 (2014) 180–185.
[24] R.O. Ocaya, A. Al-Ghamdi, F. El -Tantawy, W.A. Farooq, F. Yakuphanoglu, J. Alloy Compd. 674 (2016) 277–288, doi:http://dx.doi.org/10.1016/j.jallcom.2016.02.267.
[25] R.K. Gupta, R.A. Singh, Mater. Chem. Phys. 86 (2004) 279–283.
[26] M. Soylu, M. Cavas, A.A. Al-Ghamdi, Z.H. Gafer, F. El-Tantawy, F. Yakuphanoglu, Sol. Energy Mater. Sol. Cells 124 (2014) 180–185.
[27] B. Gunduz, A.A. Al-Ghamdi, A.A. Hendi, Z.H. Gafer, S. El-Gazzar, F. El-Tantawy, F. Yakuphanoğlu, Superlattices Microstruct. 64 (2013) 167–177.
[28] S. Karatas, A. Turut, Vacuum 74 (2004) 45.
[29] A. Tombak, Y.S. Ocak, S. Asubay, T. Kilicoglu, F. Ozkahraman, Mater. Sci. Semicond. Process. 24 (2014) 187–192.
[30] I. Dokme, S. Altindal, I. Uslu, J. Appl. Polym. Sci. 125 (2012) 1185–1192, doi:http://dx.doi.org/10.1002/app.36327.
[31] I. Dokme, S. Altindal, T. Tunc, I. Uslu, Microelectron. Reliab. 50 (2010) 39–44.
[32] E.H. Nicollian, A. Goetzberger, Bell Syst. Technol. J. 46 (1967) 1055–1133.
[33] A.N. Donald, Semiconductor physics and devices, in: C.W. Wilmsen (Ed.), Physics and Chemistry of III–V Compound Semiconductor Interface, Plenum, NewYork, 1992, pp. 1985.